Structural Mimics of the [Fe]-Hydrogenase: A Complete Set for the Group VIII Metals

*Chandan Kr Barik, Rakesh Ganguly, Yongxin Li and Weng Kee Leong**

Division of Chemistry & Biological Chemistry, Nanyang Technological University, 21 Nanyang Link, Singapore, 637371.

ABSTRACT A set of structural mimics of the [Fe]-hydrogenase active site comprising all the group VIII metals, *viz*., [M(*2*-NHC(O)C_5H_4N)$(CO)_2$(*2*-S-C_5H_4N)], has been synthesized. They exist as a mixture of isomers in solution, and the relative stability of the isomers depends on the nature of the metal and the substituent at the 6-position of the pyridine ligand.

1. INTRODUCTION

Three phylogenetically distinct types of hydrogenases, enzymes that catalyse the reversible oxidation of molecular hydrogen,[1,2] are known and they are designated as the [NiFe]-, [FeFe]- and [Fe]-hydrogenases.[3-5] The redox-active [NiFe]- and [FeFe]-hydrogenases have been the focus of attention for many years. As they catalyse the reversible interconversion of molecular hydrogen with protons and electrons, understanding their chemistry has potential impact on the so-called "hydrogen economy".[6,7] The third hydrogenase is a more recent discovery,[8] and subsequent identification of an iron centre as its active site led to its redesignation as the [Fe]-hydrogenase.[9] Unlike the other two hydrogenases, it is redox inactive and performs a different chemistry; it

catalyses the reversible, heterolytic cleavage of dihydrogen into H^+ and H^- in the presence of a particular carbocationic substrate, N^5,N^{10}-methenyltetrahydromethanopterin (methenyl-H_4MPT).[10-15] This methenyl-H_4MPT^+ reduction is an important intermediary step in the conversion of carbon dioxide to methane by methanogens grown under nickel-deficient conditions.[10]

The determination of the structure of the [Fe]-hydrogenase, and especially of its active site, involved a number of studies,[9,10,16] including several crystallographic studies.[17-20] The currently accepted configuration of the active site consists of an iron centre coordinated by a thiolate, two cis-CO, a 2-acylmethyl-6-pyridinol ligand, and an as-yet unknown ligand which is most probably a water molecule (Figure 1a). A number of molecular models which mimic the geometry of the natural [Fe]-hydrogenase have been reported, but none containing the heavier homologues ruthenium or osmium.[21-30] Given that many ruthenium and osmium complexes catalyze hydrogen activation and hydrogen transfer reactions,[31-34] it is envisaged that structural mimics containing these metals may exhibit similar activity. Furthermore, their expected greater stability compared to the iron analogues should help in studies towards a better understanding of the nature of the active site in [Fe]-hydrogenase and its catalytic action.

Although mimics containing a 2-acylmethylpyridinyl ligand may be closer structurally to the [Fe]-hydrogenase active site, there is already an elegant and accessible route to the very similar carbamoyl pyridinyl ligand.[22,35] In addition, the bidentate 2-mercaptopyridine ligand has also been shown to be an efficient way to introduce a thiolate ligand in such mimics (Figure 1b).[21,36] We therefore decided on the synthesis of a complete set of the metallacyclic carbamoyl complexes for the group VIII metals (Figure 1c), which is reported here.

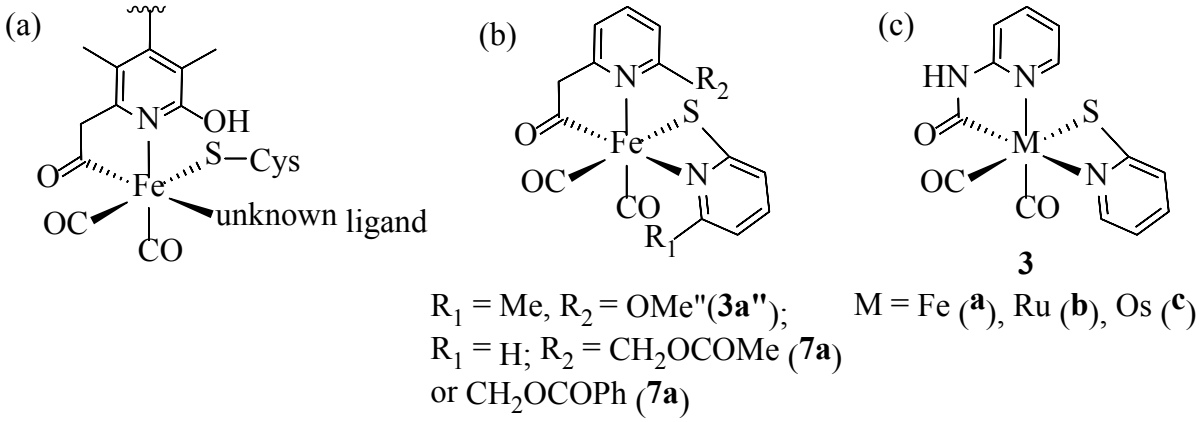

Figure 1. Structure of (a) the active site of [Fe]-hydrogenase, (b) previously reported complexes containing the 2-mercaptopyridine ligand, and (c) metallacyclic carbamoyl complexes synthesized in this study.

2. RESULTS AND DISCUSSION

2.1 Synthesis

The iron and ruthenium mimics **3a**, **3b** and **3b'** can be synthesized in two steps (Scheme 1 top). The starting complexes **1a** and **1b** are available from $Fe(CO)_5$ and $Ru_3(CO)_{12}$, respectively,[22,37] while the syntheses of **2b** and **2b'** follow that reported for **2a**. Although they are analogues to each other, the solubilities of **2b** and **2b'** are quite different; while **2b'** is soluble in acetone, **2b** is not. This synthetic route is, however, not viable for preparing the osmium analogue **3c**, which is synthesized via the trifluroacetate complex **5** instead, in 28% yield.[38,39] Changing the solvent in this latter reaction from toluene to chloroform does not improve the yield of **3c**, and the side-product **6** is also isolated (Scheme 1 bottom). The formulation of **6** has been confirmed spectroscopically and analytically, and by a single crystal X-ray diffraction study. The source of the chloride ligand is presumably the solvent ($CHCl_3$).[40] Although iron, ruthenium and rhenium

analogues are known, to the best of our knowledge, **3c** is the first example of a five-membered carbamoyl pyridinyl osmacycle.[41-43]

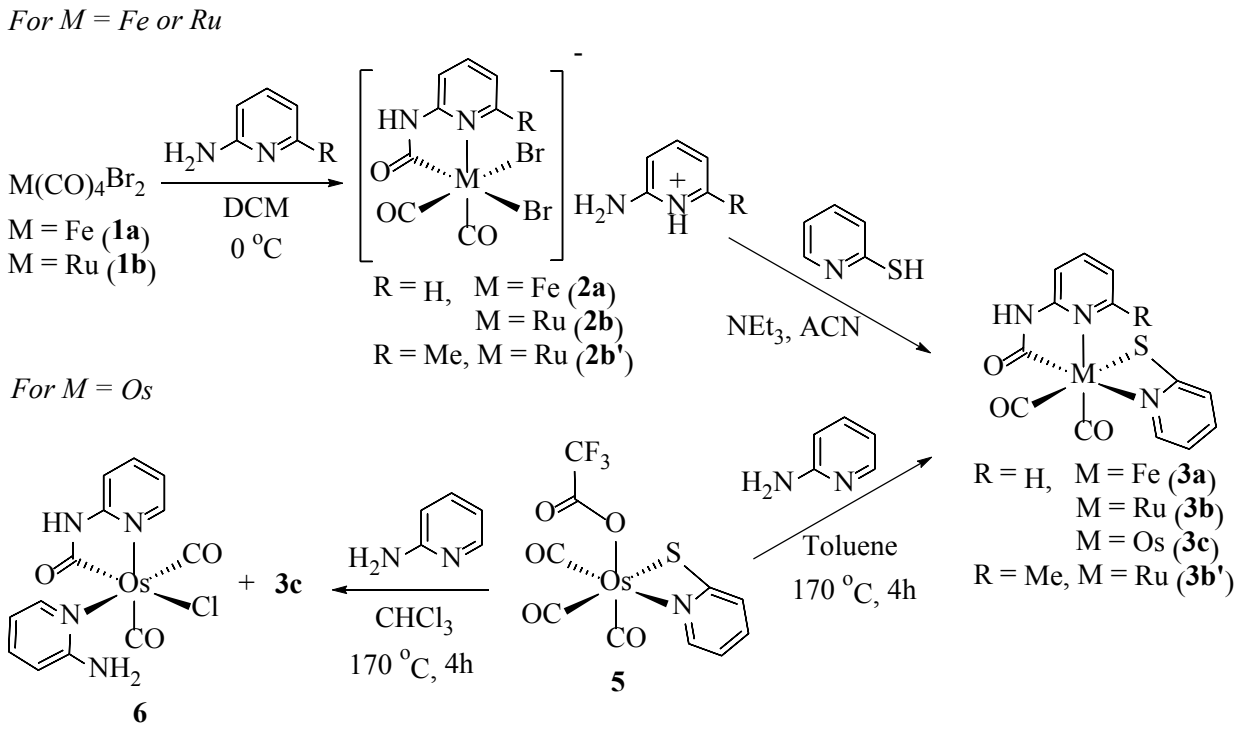

Scheme 1. Synthesis of the model complexes.

The structures of **2b** and **2b'** were confirmed by single crystal X-ray diffraction studies, although that for the latter exhibited disorder. They are isostructural with the known Fe analogue **2a**; the carbamoyl pyridinyl ligand forms a planar five-membered metallacycle with the ruthenium center, with mutually facial arrangement of three terminal bromide and carbonyl ligands. An ORTEP plot showing the molecular structure of the complex anion of **2b** is given in Figure 2, together with selected bond parameters. The Ru-Br2 bond is significantly longer than the Ru-Br1 bond ((2.6376(6) Å) and 2.5828(6) Å, respectively) and may be attributed to a stronger trans influence of the carbamoyl compared to the carbonyl ligand.[35]

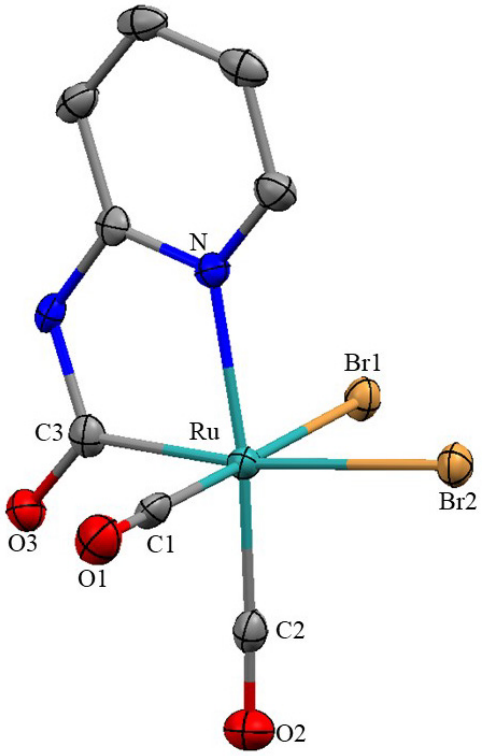

Figure 2. ORTEP plot of the anionic complex **2b**. The counter cation and all hydrogen atoms have been omitted for clarity. Thermal ellipsoids are drawn at the 50% probability level. Selected bond lengths (Å) and angles (°): Ru-N = 2.130(4), Ru-Br1 = 2.5827(6), Ru-Br2 = 2.6375(6), Ru-C1 = 1.875(5), R-C2 = 1.888(5), Ru-C3 = 2.011(5); C3-Ru-N = 79.48(17), C3-Ru-C2 = 90.6(2), C2-Ru-Br1 = 89.43(14), C3-Ru-Br1 = 85.95(13), N-Ru-Br1 = 87.64(10), C1-Ru-Br2 = 91.66(15), C2-Ru-Br2 = 96.45(14), N-Ru-Br2 = 93.26(11), Br1-Ru-Br2 = 90.213(19).

2.2 Isomerisation in solution

The situation with **3n** (where n = a, b, b' or c) is more complex. While the ^{1}H NMR spectrum of **3b'** showed two sets of resonances in an ~3:2 ratio, the spectra of freshly prepared samples of **3a-c** gave only one set of resonances but a second set slowly emerged on standing under ambient conditions; this is illustrated for **3b** in Figure 3.

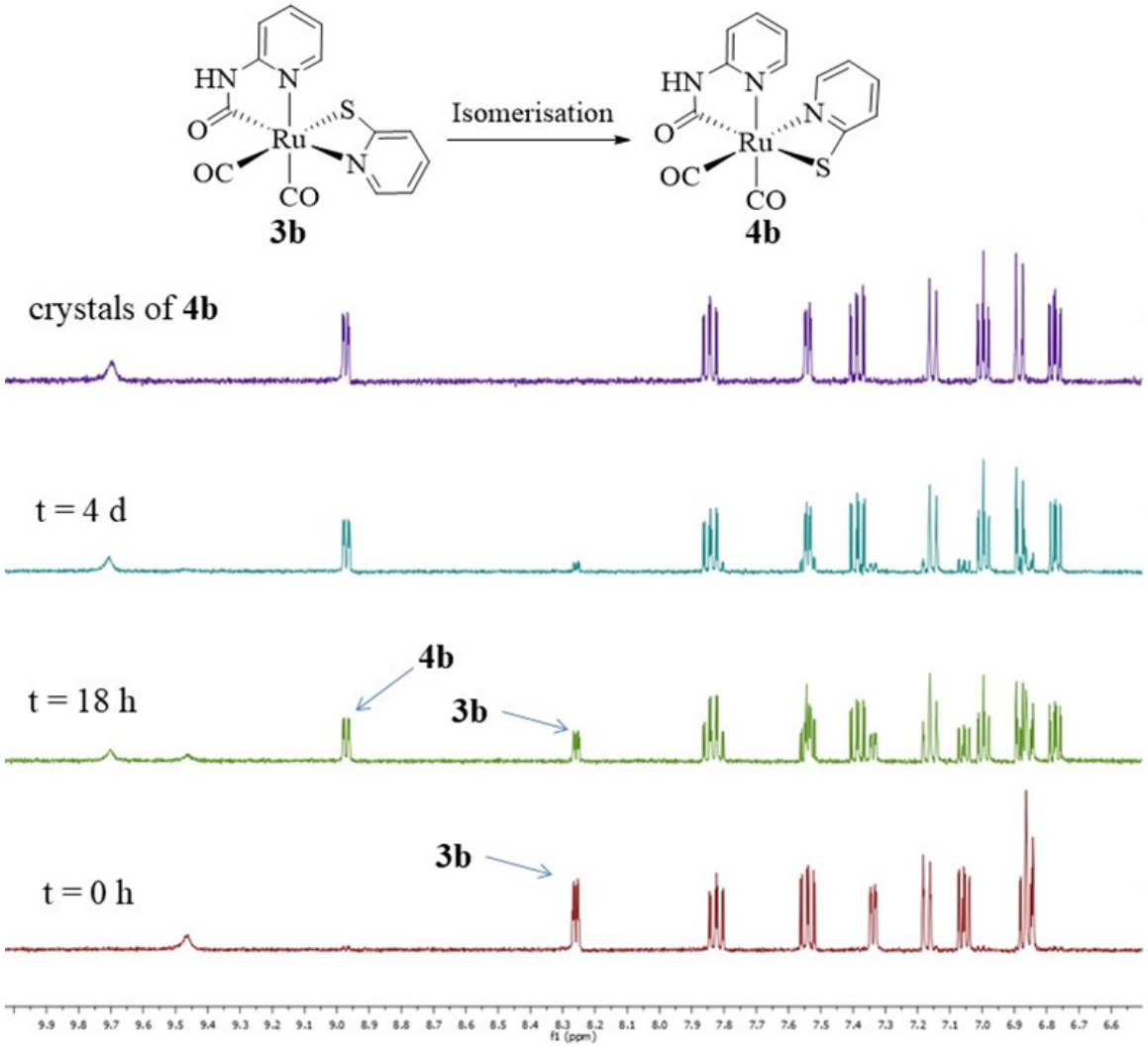

Figure 3. ^{1}H NMR spectrum of a solution (d_6-acetone) of **3b** on standing, and of crystals of **4b**.

These observations are consistent with a slow isomerization process and indeed, crystallographic structural determination carried out on crystals of **3a-c** show that while **3a** has the structure depicted in scheme 1, the ruthenium (**3b**) and osmium (**3c**) analogues are an isomeric form, *viz*., **4b** and **4c**, respectively; ORTEP plots showing their molecular structures are given in Figure S2. The ^{1}H NMR spectra of the crystals of **4b** and **4c** also correspond to those for solutions of **3b** and **3c**, respectively, which have been left to stand for a long time. The isomerization also manifested itself, albeit less distinctly, in the infrared spectra; for example, freshly prepared **3a** exhibited two CO stretches at 2037 and 1976 cm^{-1} which, upon standing for two days, shifted slightly to 2039 and 1980 cm^{-1}.

Assignment of the ^{1}H resonances to the two isomeric forms can be made as they exhibit distinct patterns. For example, the spectrum for **3b** shows a signal at 8.25 ppm which shifts downfield to 9.00 ppm upon isomerization to **4b**. In the case of the iron analogue, although resonances attributable to the isomer **4a** are observed, they broaden on standing over 2 d, indicating decomposition. The isomers of ruthenium and osmium compounds can also be separated as close-moving bands on a TLC plate, but the IR and NMR spectra of these show them to be isomeric mixtures with a constant ratio, suggesting that the isomerization is slow and reaches an equilibrium. In the case of **3'/4b'**, the signals for **4b'** appear more downfield than those of **3b'**; the assignment is made by comparison with those of [Fe(*2*-$CH_2C(O)C_5H_3N$-*6*-OMe)$(CO)_2$(*2*-SC_5H_3N-*6*-Me)] (**3"/4a"**),[21] as well as with computed chemical shift values (Table S4). A variable temperature NMR experiment conducted did not show any significant broadening even at elevated temperatures, again indicative of slow isomerization (Figure S6). Fortunately, we were able to obtain separate crystals of **3b'** and **4b'**, and confirmed their structures crystallographically; the ORTEP plots showing their molecular structures are given in Figure 4.

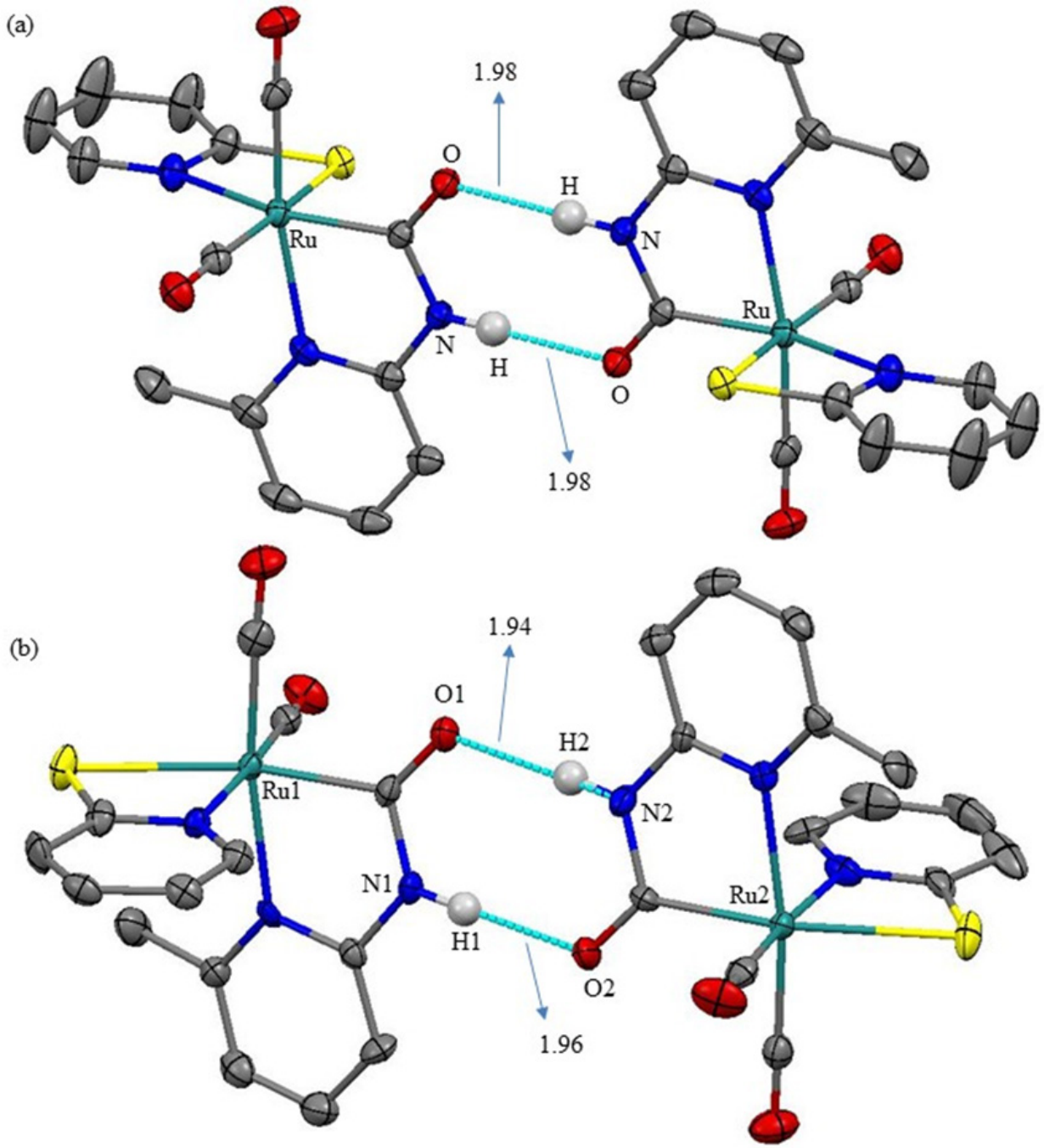

Figure 4. ORTEP plots of **3b'** (top) and **4b'** (bottom) showing hydrogen bonding between two monomeric units. All hydrogen atoms, except those involved in the hydrogen bonding, have been omitted for clarity. Thermal ellipsoids are drawn at the 50% probability level.

The isomer ratios obtained from free energy calculations for **3n** and **4n** through a computational study with M06 density functional theory are in excellent agreement with those obtained from integration of the NMR spectra; a similar set of computations with the B3LYP density functional gives free energies of similar magnitude (Table 1). The values clearly show that **4n** is more stable than **3n** for all three metals, with the difference increasing in the order: Fe < Ru < Os. The greater stability of **4n** compared to **3n** may be attributed to the preferred placement of the π-donating thiolate, rather than the π-accepting pyridine, to be trans to the strong π-acceptor carbamoyl ligand.[44] In comparison to **3/4b**, the energy gap for the 6-Me substituted analogues **3/4b'** is much smaller (-0.8 kJ/mol), suggesting that substitution at the 6-position of the pyridine ligand affects significantly the relative stability, as well as the structural parameters (Table 2), of the complexes. This steric effect is also seen in the iron complex **3a"** which has substituents at the 6-position of both the pyridine ligands; this was reported to isomerize to the corresponding **4a"** upon uv irradiation and reverted back upon removal of the irradiation.[21] In agreement with this, our computational study shows that **3a"** is much more stable (+27.0 kJ/mol) than **4a"** (Table 1).

Table 1. Computed difference in free energy with two density functionals and basis sets, and comparison of calculated and experimental isomer ratios, of complexes **3n** and **4n**.

Complex	Calculated G^{o}(**4n**) - G^{o}(**3n**) (kJ/mol)		Ratio of **3n:4n**	
	M06	B3LYP	Calculated*	Experimental
3a/4a	-3.7	-3.8	20:80	25:75
3b/4b	-4.5	-3.0	15:85	20:80
3c/4c	-5.8	-4.3	10:90	15:85
3b'/4b'	-0.8	-0.1	45:55	40:60
3a"/4a"	+27.0	-	100:0	-

*Ratio calculated from the M06 values.

The above results suggest that **3n** is the kinetic product of the reaction between **2n** and *2*-mercaptopyridine (PySH). It is proposed that initial substitution of one bromide ligand by the thiolate (PyS) afforded intermediate **A** which is preferred over its isomer **B** as this places the stronger π donor (Br > SPy) trans to the carbamoyl ligand.[45] Displacement of the second bromide ligand by the pyridyl functionality leads to **3n** (Scheme 2). In agreement with this, DFT calculation shows that **A** is more stable than **B** by 6.6 kJ/mol. While the photoisomerization of **3a"** has been proposed to occur via migratory deinsertion of the acyl ligand back to a carbonyl and an alkyl ligand following CO loss,[21] given the mild conditions (room temperature and no photochemical activation required), it is unlikely that the isomerization which we have observed follows an analogous mechanism; the well-studied Ray-Dutt twist is more likely.[46-49]

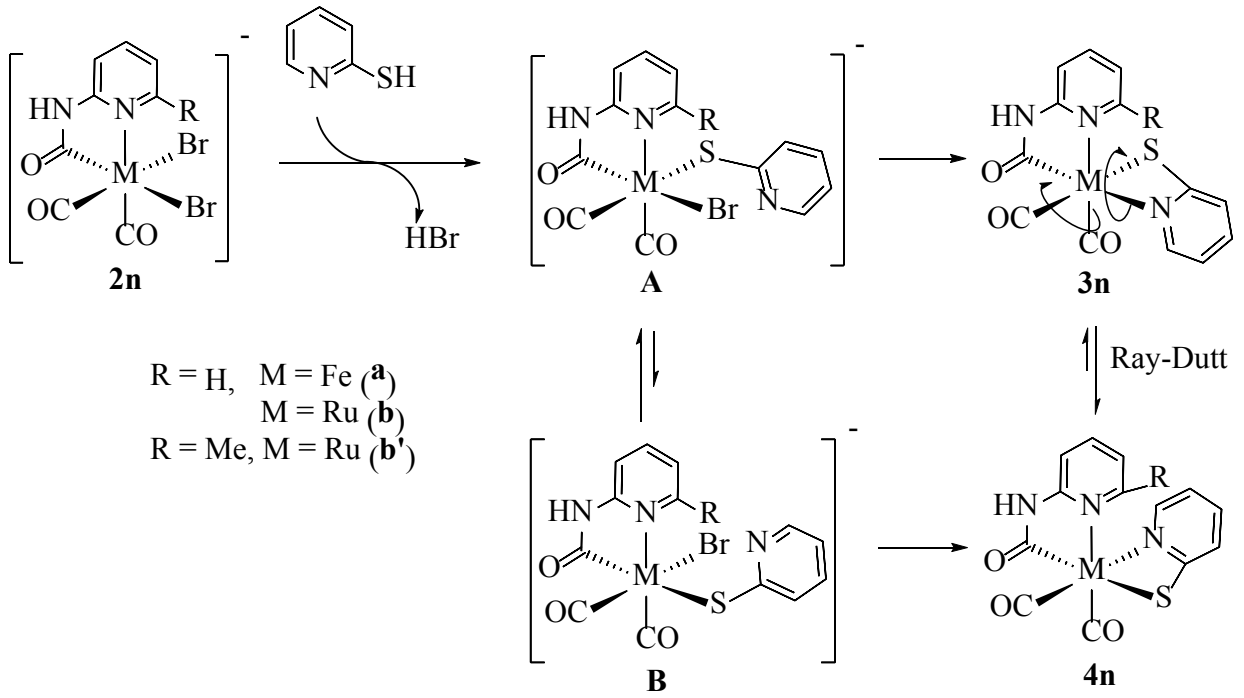

Scheme 2. Proposed pathway for the formation and isomerization of **3n** and **4n**.

2.3 Crystallographic structures of 3 and 4

The crystal structures of all the five complexes (**3a**, **4b**, **4c** and **3/4b'**) obtained show that they exist as dimers through two intermolecular hydrogen bonds between amide groups; selected bond parameters, together with a common atomic labelling scheme for the monomeric units, are collected in Table 2. The C=O···H distances of 1.88 to 2.20 Å are within the range (1.5-2.2 Å) observed for medium H-bonding interactions.[50,51] Fragments corresponding to dimeric species were also observed in the mass spectra but were absent when trifluoroacetic acid was added to the sample prior to mass spectrometry (Figure S8).

The dimers either have crystallographically imposed (**3a**, **4b** and **4c**), or near (**4b'**), centrosymmetry while each monomeric unit is chiral (Δ or Λ form). The steric effect of the 6-Me substituent in the carbamoyl pyridine ring of **3/4b'** can be seen in the longer Ru-N1 bonds compared to that in **4b**. It is also apparent from the large N2-Ru-N1 angle in **3b'** and the larger S-Ru-N1 angle in **4b'**. The stronger trans influence of the carbamoyl ligand compared to the carbonyl ligand leads to significant elongation of the M-N2 bonds over the M-N1 bonds (2.036(3) vs 1.998(2) and 2.200(2) vs 2.152(2), for **3a** and **3b'**, respectively), and for the Ru-S bond in **4b** and **4b'** compared to that in **3b'**.

Table 2. Common atom labelling scheme and selected bond parameters for the monomeric units of **3a, 4b**, **4c** and **3/4b'**. The dimeric units in **3a**, **4b**, **4c** and **3b'**, but not **4b'**, are located at crystallographic inversion centres.

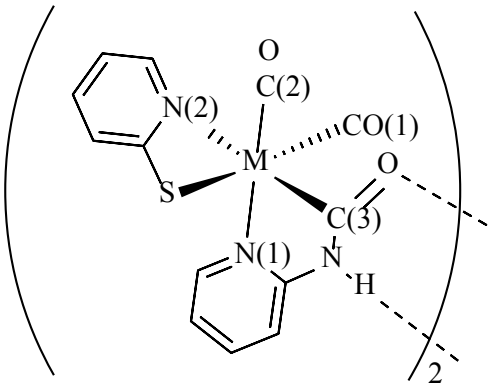

Complex **3n**

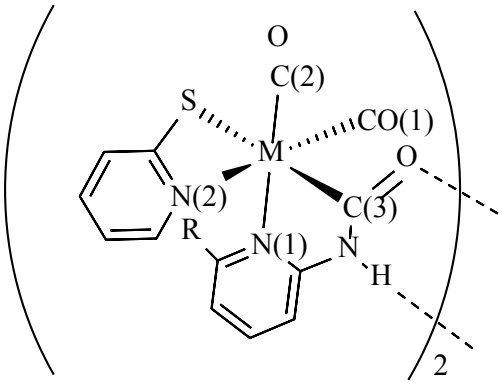

Complex **4n**

	3a	**3b'**	**4b**	**4c***	**4b'**
Bond length (Å)					
M	Fe	Ru	Ru	Os	Ru
R	H	Me	H	H	Me
C(C3)=O···H	1.93	1.98	1.88	2.07	1.94; 1.96
M-N1	1.998(2)	2.152(2)	2.114(3)	2.1178(2)	2.148(11); 2.175(10)
M-N2	2.036(3)	2.200(2)	2.116(4)	2.1409(2)	2.113(7); 2.112(9)
M-S	2.3796(10)	2.4754(6)	2.5204(11)	2.5392(3)	2.574(3); 2.569(3)
M-C1	1.774(3)	1.875(2)	1.884(5)	1.8902(2)	1.882(10); 1.891(10)
M-C2	1.785(4)	1.873(3)	1.879(4)	1.8762(2)	1.892(12); 1.878(12)
M-C3	1.935(3)	2.020(2)	2.021(4)	2.0460(2)	2.022(9); 2.027(9)
Bond angle (º)					
N1-M-C3	82.67(11)	79.28(9)	79.55(15)	82.37(1)	79.7(4); 79.4(3)
C3-M-C2	87.51(14)	90.40(10)	92.86(17)	93.61(1)	90.4(4); 91.2(4)
S-M-N1	88.84(7)	88.36(7)	94.66(9)	91.16(1)	98.0(2); 100.5(2)
S-M-N2	70.14(8)	66.63(6)	66.45(10)	64.73(1)	65.2(2); 65.5(3)
N2-M-N1	93.96(10)	101.42(8)	86.19(13)	85.19(1)	87.5(3); 88.4(3)

*The crystal exhibited disorder, modelled with two sites (~62:38 ratio). Bond parameters given are for the major part.

3. CONCLUSION

In this work, we described for the first time the synthesis of all three group VIII metal complexes of the type [M(*2*-NHC(O)C_5H_3NR)$(CO)_2$(*2*-SC_5H_4N)] (where M = Fe, Ru or Os) as structural mimics for the [Fe]-hydrogenase active site. These complexes were found to exist as isomers which differed in the relative orientation of the mercaptopyridine ligand, and their relative stability depended on both the nature of the metal, as well as to steric effects (in particular, substitution at the 6-position of the carbamoyl pyridine ligand). In the solid state, these complexes existed as dimers through intermolecular hydrogen bonding between amide groups. It may be expected that both these factors – steric interaction and hydrogen-bonding – would have implications for the design of [Fe]-hydrogenase mimics, and on protein folding if these complexes were incorporated into a protein.

4. EXPERIMENTAL SECTION

General Procedures. All experiments were performed under an argon atmosphere using standard Schlenk techniques. Chemicals were obtained from Sigma Aldrich and were used as received. The compounds **1** and **5** were synthesized according to the literature procedures.[22,37-39] Solvents that were used for reactions were distilled over the appropriate drying agents under argon before use. TLC separation were carried out on 20 x 20 cm^2 plates coated with silica gel 60 F254 from Merck. HRMS were recorded in ESI mode on a Waters UPLC-Q-Tof MS mass spectrometer. ^{1}H and $^{13}C\{^1H\}$ NMR spectra were obtained on a JEOL 400 MHz spectrometer at room temperature unless stated otherwise. Chemical shifts for ^{1}H and $^{13}C\{^1H\}$ were referenced with respect to the residual resonances of the respective deuterated solvents. Infrared spectra were recorded on a Bruker Alpha FT-IR spectrometer in a IR cell with NaCl windows and a path length of 0.1 mm at

a resolution of 2 cm^{-1}. Elemental analyses were performed on PerkinElmer 2400 Series II CHN/O Elemental Analyzer in house. Microwave synthesis were carried out on Monowave 400 reactor from Anton Paar. Electrochemical measurements were made using a computer-controlled Eco Chemie Autolab PGSTAT302N potentiostat in a three-electrode cell with a 1 mm diameter planar glassy carbon disk (Cypress Systems) working electrode, a platinum wire (Metrohm) auxiliary electrode, and a silver wire (Cypress Systems) miniature reference electrode connected to the main solution via a salt bridge containing 0.5 M *n*-Bu_4NPF_6 in MeCN. Gas chromatography measurements were made using Agilent 7890A gas-chromatograph with a thermal conductivity detector (TCD), a 5 Å molecular sieve column (2 mm × 5 m), and argon as the carrier gas.

Preparation of [$RuBr_2$(*2*-$NHC(O)C_5H_4N$)$(CO)_2$][*2*-$NH_2C_5H_4NH$] (2b). A solution of $Ru(CO)_4Br_2$ (200 mg, 0.53 mmol) and *2*-amino-pyridine (100 mg, 1.08 mmol) in dichloromethane (30 mL) were stirred for 3h at room temperature, which gave a white precipitate within few minutes. The white precipitate was separated via filtration and washed with hexane (50 mL) followed by dichloromethane (100 mL) to afford analytical pure **2b**. Yield: 164 mg, 0.31 mmol, 58%. mp 319-320 ºC. IR (MeOH, cm^{-1}): ν_{CO} 2060 (s), 1994 (s). ^1H NMR (400 MHz, CD_3OD): δ 9.16-9.14 (d, *J* = 5.0 Hz, 1H, arom-H), 8.23 (br. s, 1H, NH), 7.97-7.92 (m, 2H, arom-H), 7.85-7.84 (d, *J* = 6.4 Hz, 1H, arom-H), 7.12-7.09 (m, 2H, arom-H), 7.04-7.01 (d, J = 9.2 Hz, 1H, arom-H), 6.92-6.89 (t, *J* = 6.0 Hz, 1H, arom-H) ppm. HRMS. Calcd for $[M]^-$: *m/z* 438.7721. Found: *m/z* 438.7718. Anal. Calcd for $C_{13}H_{12}N_4O_3Br_2Ru.CH_2Cl_2$: C 27.2, H 2.3, N 9.1. Found C 27.4, H 1.8, N 8.4.

Preparation of [$RuBr_2$(*2*-$NHC(O)C_5H_3NMe$)$(CO)_2$][*2*-$NH_2C_5H_3NHMe$] (2b'). Compound **2b'** has been prepared by following an analogous procedure as that of **2b** from $Ru(CO)_4Br_2$ (200 mg, 0.53 mmol) and 2-amino-6-methylpyridine (117 mg, 1.08 mmol). In this case, the resulting

mixture was stirred for 12h at room temperature and the resulting white precipitate was purified by same way as that of **2b**. Yield: 196 mg, 0.35 mmol, 66%. mp 192-193 ^{o}C. IR (MeOH, cm^{-1}): ν_{CO} 2060 (s), 1986 (s). ^{1}H NMR (400 MHz, $(CD_3)_2CO$): δ 9.50 (br. s, 1H, NH), 7.94-7.90 (t, *J* = 9.2 Hz, 1H, arom-H), 7.70-7.66 (t, *J* = 8.2 Hz, 1H, arom-H), 7.61 (br. s, 2H, NH), 7.01-6.99 (d, *J* = 8.7 Hz, 1H, arom-H), 6.93-6.91 (d, *J* = 8.2 Hz, 1H, arom-H), 6.86-6.81 (m, 2H, arom-H), 2.95 (s, 3H, Me), 2.58 (s, 3H, Me) ppm. ^{13}C{^{1}H} NMR (400 MHz, $(CD_3)_2CO$): 158.4, 155.4, 147.1, 144.7, 139.7, 116.2, 112.2, 110.5, 106.4, 105.9, 30.9, 18.3 ppm. HRMS. Calcd for [M]$^{-}$: *m/z* 452.7878. Found: *m/z* 452.7867. Anal. Calcd for $C_{15}H_{16}N_4O_3Br_2Ru$: C 32.1, H 2.9, N 10.0. Found C 32.6, H 2.5, N 10.1.

Preparation of [Fe(*2*-NHC(O)C$_5$H$_4$N)(CO)$_2$(*2*-SC$_5$H$_4$N)] (3a). Triethylamine (0.03 mL, 0.21 mmol) and 2-mercaptopyridine (22 mg, 0.21 mmol) were added into a solution of **2a** (100 mg, 0.21 mmol) in acetonitrile (10 mL). The resulting mixture was then stirred for 1h at ambient temperature to give a brown solution. The solvent was then evaporated under vacuum. The residue was dissolved in dichloromethane (5 mL) and placed onto a neutral alumina column. Elution with dichloromethane/acetone (v/v = 20/1) developed a yellow band, which afforded **3a** as orange crystals. Yield: 27 mg, 0.08 mmol, 38%. mp 180-181 ^{o}C. IR (MeCN, cm^{-1}): ν_{CO} 2037 (s), 1976 (s). ^{1}H NMR (400 MHz, $(CD_3)_2CO$): δ 9.60 (br. s, 1H, NH), 8.32-8.31 (dd, *J* = 0.9 Hz, *J* = 5.5 Hz, 1H, arom-H), 7.84-7.78 (dt, *J* = 1.4 Hz, *J* = 7.4 Hz, 1H, arom-H), 7.60-7.56 (dt, *J* = 1.4 Hz, *J* = 7.3 Hz, 1H, arom-H), 7.24-7.23 (dd, *J* = 0.9 Hz, *J* = 5.5 Hz, 1H, arom-H), 7.18-7.16 (dd, *J* = 0.9 Hz, *J* = 8.7 Hz, 1H, arom-H), 7.12-7.09 (dt, *J* = 1.4 Hz, *J* = 6.4 Hz, 1H, arom-H), 6.89-6.86 (dt, *J* = 1.4 Hz, *J* = 6.0 Hz, 1H, arom-H), 6.82-6.80 (dd, *J* = 0.9 Hz, *J* = 8.2 Hz, 1H, arom-H) ppm. ^{13}C{^{1}H} NMR (400 MHz, $CDCl_3$): 183.5 (NHCO), 180.2 (terminal CO), 179.2 (terminal CO), 158.1, 150.5, 149.0, 145.9, 139.1, 135.8, 126.6, 118.3, 117.0, 109.5 ppm. HRMS. Calcd for [M]$^{+}$: *m/z* 452.7878.

Found: *m/z* 452.7867. Anal. Calcd for $C_{13}H_9N_3O_3SFe$: C 45.5, H 2.6, N 12.2, S 9.3. Found C 45.5, H 2.3, N 12.3, S 9.9.

Preparation of [Ru(*2*-NHC(O)C_5H_4N)$(CO)_2$(*2*-SC_5H_4N)] (3b). Triethylamine (0.03 mL, 0.21 mmol) and *2*-mercaptopyridine (22 mg, 0.21 mmol) were added into a solution of **2b** (112 mg, 0.21 mmol) in acetonitrile (30 mL). The resulting mixture was then stirred for 2h at ambient temperature. The solvent was then evaporated in vacuum. The residue was purified by TLC with dichloromethane/ethyl acetate (v/v = 8/2) as an eluent, which afforded **3b** as yellow solid. R_f = 0.56. Yield: 70 mg, 0.18 mmol, 72%. IR (MeCN, cm^{-1}): ν_{CO} 2049 (s), 1984 (s). ^1H NMR (400 MHz, $(CD_3)_2CO$): δ 9.48 (br. s, 1H, NH), 8.29-8.27 (dd, *J* = 0.9 Hz, *J* = 5.5 Hz, 1H, arom-H), 7.86-7.82 (dt, *J* = 1.4 Hz, *J* = 7.3 Hz, 1H, arom-H), 7.58-7.54 (dt, *J* = 0.9 Hz, *J* = 7.3 Hz, 1H, arom-H), 7.36-7.35 (dd, *J* = 0.9 Hz, *J* = 5.0 Hz, 1H, arom-H), 7.20-7.18 (dd, *J* = 1.4 Hz, *J* = 8.2 Hz, 1H, arom-H), 7.09-7.06 (dt, *J* = 0.9 Hz, *J* = 6.4 Hz, 1H, arom-H), 6.90-6.86 (m, 2H, arom-H) ppm. $^{13}C\{^1H\}$ NMR (400 MHz, $(CD_3)_2CO$): 202.2 (NHCO), 197.5 (terminal CO), 193.1 (terminal CO), 180.7, 158.3, 150.1, 145.6, 140.2, 136.1, 126.9, 118.1, 116.4, 109.3 ppm. HRMS. Calcd for $[M+H]^+$: *m/z* 389.9489. Found: *m/z* 389.9486. Anal. Calcd for $C_{13}H_9N_3O_3SRu.C_4H_8O_2$: C 42.9, H 3.6, N 8.8, S 6.7. Found C 43.2, H 3.5, N 8.7, S 6.1.

Preparation of [Ru(*2*-NHC(O)C_5H_4N)$(CO)_2$(*2*-SC_5H_4N)] (4b). A sample of **3b** (20 mg) was dissolved in tetrahydrofuran (2 mL) and kept the resultant solution at room temperature for 2 d which afforded yellow crystals of **4b** suitable for x-ray diffraction study. IR (MeCN, cm^{-1}): ν_{CO} 2050 (s), 1984 (s). ^1H NMR (400 MHz, $(CD_3)_2CO$): δ 9.76 (br. s, 1H, NH), 9.00-8.98 (dd, *J* = 0.9 Hz, *J* = 5.0 Hz, 1H, arom-H), 7.89-7.84 (dt, *J* = 1.4 Hz, *J* = 5.5 Hz, 1H, arom-H), 7.57-7.55 (dd, *J* = 0.9 Hz, *J* = 5.5 Hz, 1H, arom-H), 7.43-7.39 (dt, *J* = 0.9 Hz, *J* = 7.3 Hz, 1H, arom-H), 7.21-7.16 (dd, *J* = 1.4 Hz, *J* = 8.7 Hz, 1H, arom-H), 7.04-7.00 (dt, *J* = 1.4 Hz, *J* = 6.0 Hz, 1H, arom-H), 6.92-

6.87 (dd, *J* = 0.9 Hz, *J* = 8.2 Hz, 1H, arom-H), 6.81-6.78 (dt, *J* = 1.8 Hz, *J* = 5.5 Hz, 1H, arom-H) ppm. $^{13}C\{^{1}H\}$ NMR (400 MHz, $(CD_3)_2CO$): 201.6 (NHCO), 198.4 (terminal CO), 196.7 (terminal CO), 182.0, 158.4, 148.1, 148.0, 141.0, 136.5, 128.1, 117.4, 116.5, 109.2 ppm.

Preparation of [Ru(*2*-NHC(O)C$_5$H$_3$NMe)(CO)$_2$(*2*-SC$_5$H$_4$N)] (3b'). An analogous procedure as that of **3b** was followed for the synthesis of **3b'** from **2b'** (118 mg, 0.21 mmol); which obtained as a mixture of **3b'** and **4b'**. mp 210-211 ºC. IR (MeCN, cm^{-1}): ν_{CO} 2050 (s), 1983 (s), 1634 (m). ^{1}H NMR (400 MHz, $(CD_3)_2CO$): δ 9.72 (br. s, 1H, NH), 9.46 (br. s, 1H, NH), 8.32-8.31 (dd, *J* = 0.9 Hz, *J* = 5.5 Hz, 1H, arom-H), 7.75-7.72 (dd, *J* = 0.9 Hz, *J* = 5.9 Hz, 1H, arom-H), 7.70-7.66 (m, 2H, arom-H), 7.52-7.48 (dt, 1H, arom-H), 7.43-7.38 (dt, 1H, arom-H), 7.00-6.96 (m, 3H, arom-H), 6.92-6.76 (m, 5H, arom-H), 3.05 (s, 3H, Me), 2.13 (s, 3H, Me) ppm. ^{13}C NMR (400 MHz, $(CD_3)_2CO$): 201.6 (NHCO), 199.7 (NHCO), 197.6 (terminal CO), 196.9 (terminal CO), 183.4 (terminal CO), 182.9 (terminal CO), 159.4, 159.1, 151.7, 150.7, 148.5, 148.2, 141.9, 140.7, 137.1, 136.6, 128.9, 128.7, 127.8, 127.1, 118.5, 118.1, 117.9, 117.4, 110.1, 107.8, 28.4, 26.1 ppm. HRMS. Calcd for $[M+H]^+$: *m/z* 403.9643. Found: *m/z* 403.9625. Anal. Calcd for $C_{14}H_{11}N_3O_3SRu$: C 41.8, H 2.8, N 10.4, S 8.0. Found C 41.8, H 2.4, N 10.6, S 8.6.

Preparation of [Os(*2*-NHC(O)C$_5$H$_4$N)(CO)$_2$(*2*-SC$_5$H$_4$N)] (3c). A sample of **5** (50 mg, 0.10 mmol), *2*-aminopyridine (10 mg, 0.10 mmol) and toluene (10 ml) were placed into a 30 mL microwave vial. The vial was sealed and then subjected to microwave radiation at a holding temperature of 170 ºC for 4 h, to afford a pale-yellow solution. The solvent was then evaporated under vacuum. The residue was purified by TLC with dichloromethane/ethyl acetate (v/v = 6:4) as an eluent, which afforded **3c** as yellow solid. R_f = 0.62. Yield: 13 mg, 0.03 mmol, 28%. IR (MeCN, cm^{-1}): ν_{CO} 2032 (s), 1957 (s). ^{1}H NMR (400 MHz, $(CD_3)_2CO$): δ 9.64 (br. s, 1H, NH), 8.40-8.38 (dd, *J* = 0.9 Hz, *J* = 4.6 Hz, 1H, arom-H), 7.87-7.84 (dt, *J* = 1.4 Hz, *J* = 7.4 Hz, 1H,

arom-H), 7.65-7.61 (dt, *J* = 0.9 Hz, *J* = 8.2 Hz, 1H, arom-H), 7.33-7.31 (dd, *J* = 0.9 Hz, *J* = 5.9 Hz, 1H, arom-H), 7.27-7.24 (dd, *J* = 0.9 Hz, *J* = 4.6 Hz, 1H, arom-H), 7.22-7.18 (dt, *J* = 0.9 Hz, *J* = 7.3 Hz, 1H, arom-H), 6.91-6.85 (dt, *J* = 0.9 Hz, *J* = 7.3 Hz, 1H, arom-H), 6.82-6.79 (dd, *J* = 0.9 Hz, *J* = 8.2 Hz, 1H, arom-H) ppm. HRMS. Calcd for $[M+H]^+$: *m/z* 480.0058. Found: *m/z* 480.0012. An analogous experiment in chloroform (10 mL) afforded, after TLC separation, **6** as a light yellow, crystalline solid. R_f = 0.48. Yield: 15 mg, 0.03 mmol, 30%. IR (MeCN, cm^{-1}): ν_{CO} 2041 (s), 1967 (s). ^1H NMR (400 MHz, $(CD_3)_2CO$): 9.93 (br. s, 1H, NH), 9.17-9.15 (d, *J* = 5.9 Hz, 1H, arom-H), 8.08-8.06 (d, *J* = 6.4 Hz, 1H, arom-H), 8.00-7.95 (m, 1H, arom-H), 7.50-7.46 (m, 1H, arom-H), 7.27-7.21 (m, 1H, arom-H), 7.05 (br, 2H, NH), 6.77-6.75 (d, *J* = 8.7 Hz, 2H, arom-H), 6.49-6.46 (m, 1H, arom-H) ppm. $^{13}C\{^1H\}$ NMR (400 MHz, $(CD_3)_2CO$): 189.6, 180.5, 176.7, 162.8, 159.8, 148.6, 145.9, 141.8, 139.3, 117.0, 113.1, 111.9, 109.2 ppm. HRMS. Calcd for $[M+H]^+$: *m/z* 499.0213. Found: *m/z* 499.0197. Anal. Calcd for $C_{13}H_{11}ClN_4O_3SOs$: C 31.4, H 2.2, N 11.3. Found C 31.9, H 2.0, N 11.5.

Preparation of [Os(*2*-NHC(O)C$_5$H$_4$N)(CO)$_2$(*2*-SC$_5$H$_4$N)] (4c). A sample of **3c** (10 mg) was dissolved in dichloromethane and kept the resultant solution at 0 ^oC for 2 d, which afforded crystals of **4c** suitable for x-ray diffraction study. IR (MeCN, cm^{-1}): ν_{CO} 2032 (s), 1958 (s). ^1H NMR (400 MHz, $(CD_3)_2CO$): δ 9.85 (br. s, 1H, NH), 9.07-9.05 (dd, *J* = 0.9 Hz, *J* = 5.0 Hz, 1H, arom-H), 7.90-7.86 (dt, *J* = 0.9 Hz, *J* = 7.4 Hz, 1H, arom-H), 7.69-7.67 (dd, *J* = 0.9 Hz, *J* = 4.6 Hz, 1H, arom-H), 7.50-7.46 (dt, *J* = 0.9 Hz, *J* = 7.3 Hz, 1H, arom-H), 7.24-7.22 (dd, *J* = 0.9 Hz, *J* = 8.2 Hz, 1H, arom-H), 7.03-7.00 (dt, *J* = 0.9 Hz, *J* = 8.2 Hz, 1H, arom-H), 6.93-6.89 (dt, *J* = 1.4 Hz, *J* = 7.3 Hz, 1H, arom-H), 6.84-6.82 (dd, *J* = 0.9 Hz, *J* = 8.6 Hz, 1H, arom-H) ppm. $^{13}C\{^1H\}$ NMR (400 MHz, $CDCl_3$): 193.4 (NHCO), 182.5 (terminal CO), 178.8 (terminal CO), 177.6, 168.9, 148.4, 147.5, 140.8, 136.0, 129.7, 117.8, 116.9, 108.6 ppm.

Crystallographic studies. Diffraction-quality crystals were grown from methanol (**2b** and **2b'**), acetone/dichloromethane (**3a**), acetonitrile (**3b'**), tetrahydrofuran (**4b** and **4c**) or dichloromethane/ethyl acetate (**4b'**) and mounted on quartz fibers. X-ray diffraction data were collected at 103(2) K on a Bruker X8 APEX system, using Mo Kα radiation, with the SMART suite of programs.[52] Data processing and correction were made for Lorentz and polarization effects with SAINT,[53] and for adsorption effects with SADABS.[54] Structural solution and refinement were carried out with the SHELXTL suite of programs.[55] The structures were solved by direct methods to locate the heavy atoms, followed by successive difference maps for the light, non-hydrogen atoms. The crystal of **2b'** exhibited disorder in both the cation and anion. This was modelled as disorder of both the Br ligands for the metal complex anion, and for the complete counterion, with two alternative sites each and their occupancies summed to unity. The crystal of **4c** also exhibited disorder of both the organic ligands, which were treated similarly. THF solvates were found for **4b** and **4c**; that in the latter exhibited disorder which was modeled with two sites of equal occupancy (0.35 each). Appropriate restraints were placed on all disordered parts. All non-hydrogen atoms were refined with anisotropic displacement parameters in the final model. All the organic hydrogen atoms were placed in calculated positions and refined with a riding model. The crystallographic data are summarized in Tables S1 and S2.

Computational studies. The computational studies were carried out using density function theory (DFT), utilizing the hybrid functional of Truhlar and Zhao (M06), or Beck's three-parameter hybrid function and Lee-Yang-Parr's gradient-corrected correlation function (B3LYP).[56,57] The basis set used was def2TZVP and LanL2DZ for M06 and B3LYP density functional, respectively,[58,59] for the transition metals, and 6-311+G(2d, p) for the light atoms for both the density functional. For calculations involving solvated species, the polarized continuum model

(PCM) was employed. Spin-restricted calculations were used for structural optimization, harmonic frequency calculations and to evaluate zero-point energy (ZPE) corrections. Optimized geometries were characterized as equilibrium structures with all real frequencies. All calculations were performed using the Gaussian 09 suite of programs.[60] The coordinates for parent complexes were taken from the crystal structure and each of the other isomers was modified from this.

AUTHOR INFORMATION

*E-mail: chmlwk@ntu.edu.sg

SUPPORTING INFORMATION

CCDC 1819192-9 contain the supplementary crystallographic data for the structures reported. These are available from the Cambridge Crystallographic Data Centre. NMR spectra showing isomerization, CVs, crystallographic tables, and optimized geometry of computed structures. This material is available free of charge via the Internet at http:// pubs.acs.org.

ACKNOWLEDGEMENTS

This work was supported by Nanyang Technological University and the Ministry of Education (Research Grant No. M4011793). CKB is grateful to the university for a Research Scholarship.

5. REFERENCES

(1) Stephenson, M.; Stickland, L. H. Hydrogenase: A Bacterial Enzyme Activating Molecular Hydrogen. *Biochem. J.* **1931**, *25*, 205-214.

(2) Elsden, S. R. Hydrogenase 1931-1981. *Trends Biochem. Sci.* **1981**, *6*, 251-253.

(3) Frey, M. Hydrogenases: Hydrogen-Activating Enzymes. *Chembiochem* **2002**, *3*, 153-160.

(4) Vignais, P. M.; Billoud, B.; Meyer, J. Classification and Phylogeny of Hydrogenases. *FEMS Microbiol. Rev.* **2001**, *25*, 455-501.

(5) Zirngibl, C.; Hedderich, R.; Thauer, R. N^5, N^{10}-Methylenetetrahydromethanopterin Dehydrogenase from Methanobacterium Thermoautotrophicum has Hydrogenase Activity. *FEBS Lett.* **1990**, *261*, 112-116.

(6) Madden, C.; Vaughn, M. D.; Díez-Pérez, I.; Brown, K. A.; King, P. W.; Gust, D.; Moore, A. L.; Moore, T. A. Catalytic Turnover of [FeFe]-Hydrogenase Based on Single-Molecule Imaging. *J. Am. Chem. Soc.* **2011**, *134*, 1577-1582.

(7) Kim, D.-H.; Kim, M.-S. Hydrogenases for Biological Hydrogen Production. *Bioresour. Technol.* **2011**, *102*, 8423-8431.

(8) Shima, S.; Thauer, R. K. A Third Type of Hydrogenase Catalyzing H_2 Activation. *Chem. Rec.* **2007**, *7*, 37-46.

(9) Lyon, E. J.; Shima, S.; Buurman, G.; Chowdhuri, S.; Batschauer, A.; Steinbach, K.; Thauer, R. K. UV-A/blue-light Inactivation of the 'Metal-free' Hydrogenase (Hmd) from Methanogenic Archaea. *FEBS J.* **2004**, *271*, 195-204.

(10) Thauer, R. K.; Klein, A. R.; Hartmann, G. C. Reactions with Molecular Hydrogen in Microorganisms: Evidence for a Purely Organic Hydrogenation Catalyst. *Chem. Rev.* **1996**, *96*, 3031-3042.

(11) Corr, M. J.; Roydhouse, M. D.; Gibson, K. F.; Zhou, S-Z.; Kennedy, A. R.; Murphy, J. A. Amidine Dications as Superelectrofiles. *J. Am. Chem. Soc.* **2009**, *131*, 17980-17985.

(12) Corr, M. J.; Gibson, K. F.; Kennedy, A. R.; Murphy, J. A. Amidine Dications: Isolation and [Fe]-Hydrogenase-Related Hydrogenation. *J. Am. Chem. Soc.* **2009**, *131*, 9174-9175.

(13) Kalz, K. F.; Brinkmeier, A.; Dechert, S.; Mata, R. A.; Meyer, F. Functional Model for the [Fe]-Hydrogenase Inspired by the Frustrated Lewis Pair Concept. *J. Am. Chem. Soc.* **2014**, *136*, 16626-16634.

(14) Hu, B.; Chen, D.; Hu, X. Synthesis and Reactivity of Mononuclear Iron Models of [Fe]-Hydrogenase that Contain an Acylmethylpyridinol Ligand. *Chem. Eur. J.* **2014**, *20*, 1677-1682.

(15) Seo, J.; Manes, T. A.; Rose, M. J. Structural and Functional Synthetic Model of Monoiron Hydrogenase Featuring an Anthracene Scaffold. *Nat. Chem.* **2017**, *9*, 552-557.

(16) Lyon, E. J.; Shima, S.; Boecher, R.; Thauer, R. K.; Grevels, F.-W.; Bill, E.; Roseboom, W.; Albracht, S. P. Carbon Monoxide as an Intrinsic Ligand to Iron in the Active Site of the Iron-Sulfur-Cluster-free Hydrogenase H_2-Forming Methylenetetrahydromethanopterin Dehydrogenase as Revealed by Infrared Spectroscopy. *J. Am. Chem. Soc.* **2004**, *126*, 14239-14248.

(17) Shima, S.; Pilak, O.; Vogt, S.; Schick, M.; Stagni, M. S.; Meyer-Klaucke, W.; Warkentin, E.; Thauer, R. K.; Ermler, U. The Crystal Structure of [Fe]-Hydrogenase Reveals the Geometry of the Active Site. *Science* **2008**, *321*, 572-575.

(18) Shima, S.; Lyon, E. J.; Thauer, R. K.; Mienert, B.; Bill, E. Mossbauer Studies of the Iron-Sulfur Cluster-free Hydrogenase: The Electronic State of the Mononuclear Fe Active Site. *J. Am. Chem. Soc.* **2005**, *127*, 10430-10435.

(19) Hiromoto, T.; Ataka, K.; Pilak, O.; Vogt, S.; Stagni, M. S.; Meyer-Klaucke, W.; Warkentin, E.; Thauer, R. K.; Shima, S.; Ermler, U. The Crystal Structure of C176A Mutated [Fe]-Hydrogenase Suggests an Acyl-Iron Ligation in the Active Site Iron Complex. *FEBS Lett.* **2009**, *583*, 585-590.

(20) Tard, C.; Pickett, C. J. Structural and Functional Analogues of the Active Sites of the [Fe]-[NiFe]-, and [FeFe]-Hydrogenases. *Chem. Rev.* **2009**, *109*, 2245-2274.

(21) Chen, D.; Scopelliti, R.; Hu, X. [Fe]-Hydrogenase Models Featuring Acylmethylpyridinyl Ligands. *Angew. Chem., Int. Ed.* **2010**, *49*, 7512-7515.

(22) Turrell, P. J.; Wright, J. A.; Peck, J. N.; Oganesyan, V. S.; Pickett, C. J. The Third Hydrogenase: A Ferracyclic Carbamoyl with Close Structural Analogy to the Active Site of Hmd. *Angew. Chem., Int. Ed.* **2010**, *49*, 7508-7511.

(23) Xu, T.; Yin, C.-J. M.; Wodrich, M. D.; Mazza, S.; Schultz, K. M.; Scopelliti, R.; Hu, X. A Functional Model of [Fe]-Hydrogenase. *J. Am. Chem. Soc.* **2016**, *138*, 3270-3273.

(24) Shima, S.; Chen, D.; Xu, T.; Wodrich, M. D.; Fujishiro, T.; Schultz, K. M.; Kahnt, J.; Ataka, K.; Hu, X. Reconstitution of [Fe]-Hydrogenase using Model Complexes. *Nat. Chem.* **2015**, *7*, 995-1002.

(25) Xie, Z.-L.; Durgaprasad, G.; Ali, A. K.; Rose, M. J. Substitution Reactions of Iron(II) Carbamoyl-thioether Complexes Related to Mono-iron Hydrogenase. *Dalton Trans.* **2017**, *46*, 10814-10829.

(26) Royer, A. M.; Rauchfuss, T. B.; Gray, D. L. Oxidative Addition of Thioesters to Iron(0): Active-Site Models for Hmd, Nature's Third Hydrogenase. *Organometallics* **2009**, *28*, 3618-3620.

(27) Chen, D.; Scopelliti, R.; Hu, X. Synthesis and Reactivity of Iron Acyl Complexes Modeling the Active Site of [Fe]-Hydrogenase. *J. Am. Chem. Soc.* **2009**, *132*, 928-929.

(28) Wright, J. A.; Turrell, P. J.; Pickett, C. J. The Third Hydrogenase: More Natural Organometallics. *Organometallics* **2010**, *29*, 6146-6156.

(29) Song, L-C.; Zhu, L.; Hu, F-Q.; Wang, Y-X. Studies on Chemical Reactivity and Electrocatalysis of Two Acylmethyl(hydroxymethyl)pyridine Ligand-Containing [Fe]-Hydrogenase Models (2-$COCH_2$-6-$HOCH_2C_5H_3N$)$Fe(CO)_2L$ (L = η^1-SCOMe, η^1-2-SC_5H_4N). *Inorg. Chem.* **2017**, *56*, 15216-15230.

(30) Song, L-C.; Xu, K-K.; Han, X-F.; Zhang, J-W. Synthesis and Structural Studies of 2-Acylmethyl-6-Difunctionalized Pyride Ligand-Containing Iron Complexes Related to [Fe]-Hydrogenase. *Inorg. Chem.* **2016**, *55*, 1258-1269.

(31) Rohmann, K.; Kothe, J.; Haenel, M. W.; Englert, U.; Hölscher, M.; Leitner, W. Hydrogenation of CO_2 to Formic Acid with a Highly Active Ruthenium Acriphos Complex in DMSO and DMSO/Water. *Angew. Chem., Int. Ed.* **2016**, *55*, 8966-8969.

(32) Naziruddin, A. R.; Huang, Z.-J.; Lai, W.-C.; Lin, W.-J.; Hwang, W.-S. Ruthenium(II) Carbonyl Complexes bearing CCC-pincer bis-(carbene) Ligands: Synthesis, Structures and Activities Toward Recycle Transfer Hydrogenation Reactions. *Dalton Trans.* **2013**, *42*, 13161-13171.

(33) Bolano, T.; Esteruelas, M. A.; Fernandez, I.; Onate, E.; Palacios, A.; Tsai, J.-Y.; Xia, C. Osmium(II)-Bis(dihydrogen) Complexes Containing C_{aryl},C_{NHC}-Chelate Ligands: Preparation, Bonding Situation, and Acidity. *Organometallics* **2015**, *34*, 778-789.

(34) Sullivan, B. P.; Caspar, J. V.; Meyer, T. J.; Johnson, S. Hydrido Carbonyl Complexes of Osmium(II) and Ruthenium(II) Containing Polypyridyl Ligands. *Organometallics* **1984**, *3*, 1241-1251.

(35) Turrell, P. J.; Hill, A. D.; Ibrahim, S. K.; Wright, J. A.; Pickett, C. J. Ferracyclic Carbamoyl Complexes Related to the Active Site of [Fe]-Hydrogenase. *Dalton Trans.* **2013**, *42*, 8140-8146.

(36) Song, L.-C.; Hu, F.-Q.; Wang, M.-M.; Xie, Z.-J.; Xu, K.-K.; Song, H.-B. Synthesis, Structural Characterization, and Some Properties of 2-acylmethyl-6-ester Group-difunctionalized Pyridine-containing Iron Complexes Related to the Active Site of the [Fe]-Hydrogenase. *Dalton Trans.* **2014**, *43*, 8062-8071.

(37) Johnson, B.; Johnston, R.; Lewis, J. Chemistry of Polynuclear Compounds. Part XV. Halogenocarbonyl Ruthenium Compounds. *J. Chem. Soc. A*. **1969**, 792-797.

(38) Deeming, A. J.; Randle, N. P.; Bates, P. A.; Hursthouse, M. B. Protonation *versus* Oxidation in the Reaction of Trifluoroacetic Acid with Dinuclear Osmium(I) Complexes: Molecular Structure of $[Os_2(MeCO_2)_2(\mu\text{-}H)(CO)_4(PMe_2Ph)_2][PF_6]$. *J. Chem. Soc., Dalton Trans.* **1988**, 2753-2757.

(39) Deeming, A. J.; Meah, M. N.; Randle, N. P.; Hardcastle, K. I. Stepwise Conversion of $[Os(CF_3CO_2)_2(CO)_4]$ into $[Os(pyS)_2(CO)_2]$: X-ray Crystal Structures of the Complexes

[$Os(pyS)_2(CO)_x$] where x = 2 or 3 and pyS is the Pyridine-2-thionato Ligand. *J. Chem. Soc., Dalton Trans.* **1989**, 2211-2216.

(40) Doherty, S.; Newman, C. R.; Hardacre, C.; Nieuwenhuyzen, M.; Knight, J. G. Ruthenium Complexes of the 1,4-Bis(diphenylphosphino)-1,3-butadiene, Bridged Diphosphine 1,2,3,4-Me4-NUPHOS: Solvent-Dependent Interconversion of Four- and Six-Electron Donor Coordination and Transfer Hydrogenation Activity. *Organometallics* **2003**, *22*, 1452-1462.

(41) Zuo, J. L.; Fu, W. F.; Che, C. M.; Cheung, K. K. Synthesis, Crystal Structure, and Photoluminescent Properties of a Tetracarbonyl(naphthyridylcarbamoyl)rhenium(I) Complex and a Highly Emissive Tetracarbonyl(naphthyridylamido)rhenium(I) complex. *Eur. J. Inorg. Chem.* **2003**, 255-262.

(42) Nombel, P.; Lugan, N.; Donnadieu, B.; Lavigne, G. Cluster-Mediated Conversion of Diphenylacetylene into α-phenylcinnamaldehyde. Construction of a Catalytic Hydroformylation Cycle Based on Isolated Intermediates. *Organometallics* **1999**, *18*, 187-196.

(43) Tomon, T.; Koizumi, T. a.; Tanaka, K. Electrochemical Hydrogenation of $[Ru(bpy)_2(napy\text{-}\kappa N)(CO)]^{2+}$: Inhibition of Reductive Ru-CO Bond Cleavage by a Ruthenacycle. *Angew. Chem., Int. Ed.* **2005**, *44*, 2229-2232.

(44) Park, S. -H.; Milletti, M. C.; Gardner, N. Theoretical Investigation of the π-bonding Ability of P-, S-, and N-containing Ligands in Group 6 Transition Metal Complexes. *Polyhedron*, **1998**, *17*, 1267-1273.

(45) Ishii, T.; Tsuboi, S.; Sakane, G.; Yamashita, M.; Breedlove, B. K. Universal Spectrochemical series of Six-coordinate Octahedral Metal Complexes for Modifying the Ligand Field Splitting. *Dalton Trans.* **2009**, *4*, 680-687.

(46) Ashby, M. T.; Govindan, C. N.; Grafton, A. K. Kinetics and Mechanism of the Facile Diastereomeric Isomerization of a Tris(bidentate)ruthenium(II) Complex Bearing a Misdirected Bipyridyl Ligand: Δ/Λ-(δ/λ-l,l'-Biisoquinoline)bis(2,2'-bipyridine)ruthenium(II). *Inorg. Chem.* **1993**, *32*, 3803-3804.

(47) Liu, C.; Peck, J. N. T.; Wright, J. A.; Pickett, C. J.; Hall, M. B. Density Functional Calculations on Protonation of the [FeFe]-Hydrogenase Model Complex $Fe_2(\mu\text{-pdt})(CO)_4(PMe_3)_2$ and Subsequent Isomerization Pathways. *Eur. J. Inorg. Chem.* **2011**, *7*, 1080-1093.

(48) Soubra, C.; Oishi, Y.; Albright, T. A.; Fujimoto, H. Intramolecular Rearrangements in Six-Coordinate Ruthenium and Iron Dihydrides. *Inorg. Chem.* **2001**, *40*, 620-627.

(49) Hansen, L. M.; Marynick, D. S. Theoretical Study of the Intramolecular Cis-Trans Isomerization Mechanism in $Cr(CO)_5X$ (X = CO, PH, PPh_3). *Inorg. Chem.* **1990**, *29*, 2482-2486.

(50) Gilli, P.; Pretto, L.; Bertolasi, V.; Gilli, G. Predicting Hydrogen-Bond Strengths from Acid-Base Molecular Properties: The pK_a Slide Rule: Toward the Solution of a Long-Lasting Problem. *Acc. Chem. Res.* **2008**, *42*, 33-44.

(51) Jeffrey, G. A.; Takagi, S. Hydrogen-bond Structure in Carbohydrate Crystals. *Acc. Chem. Res.* **1978**, *11*, 264-270.

(52) *SMART* version 5.628; Bruker AXS Inc.: Madison, WI, USA, 2001..

(53) SAINT+ version 6.22a; Bruker AXS Inc., Wisconsin, USA, Madison, 2001.

(54) Sheldrick, G. M. *SADABS*; 1996.

(55) *SHELXTL* version 5.1; Bruker AXS Inc.: Madison, WI, USA, 1997.

(56) Zhao, Y.; Truhlar, D. G. The M06 suite of density functionals for main group thermochemistry, thermochemical kinetics, noncovalent interactions, excited states, and transition elements: two new functionals and systematic testing of four M06-class functionals and 12 other functionals. *Theor. Chem. Acc.* **2008**, *120*, 215-241.

(57) Lee, C.; Yang, W.; Parr, R. G. Development of the Colle-Salvetti Correlation-energy Formula into a Functional of the Electron Density. *Phys. Rev. B: Condens. Matter Mater. Phys.* **1988**, *37*, 785-789.

(58) (a) Gaussian Basis Sets for Molecular Calculations; Huzinaga, S.; Andzelm, J., Eds.; Elsevier: Amsterdam, 1984; p 23. (b) Ehlers, A. W.; Böhme, M.; Dapprich, S.; Gobbi, A.; Höllwarth, A.; Jonas, V.; Köhler, K. F.; Stegmann, R.; Veldkamp, A.; Frenking, G. A Set of f-polarization Functions for Pseudo-potential basis sets of the Transition Metals Sc-Cu, Y-Ag and La-Au. *Chem. Phys. Lett.* **1993**, *208*, 111-114.

(59) Adamo, C.; Barone, V. Exchange functionals with improved long-range behavior and adiabatic connection methods without adjustable parameters: The mPW and mPW1PW models. *J. Chem. Phys.* **1998**, *108*, 664-675.

(60) Frisch, M. J.; Trucks, G. W.; Schlegel, H. B.; Scuseria, G. E.; Robb, M. A.; Cheeseman, J. R.; Scalmani, G.; Barone, V.; Mennucci, B.; Petersson, G. A.; Nakatsuji, H.; Caricato, M.; Li, X.; Hratchian, H. P.; Izmaylov, A. F.; Bloino, J.; Zheng, G.; Sonnenberg, J. L.; Hada, M.; Ehara, M.; Toyota, K.; Fukuda, R.; Hasegawa, J.; Ishida, M.; Nakajima, T.; Honda, Y.; Kitao, O.; Nakai, H.; Vreven, T.; Montgomery, J. A., Jr.; Peralta, J. E.; Ogliaro, F.; Bearpark, M.; Heyd, J. J.; Brothers, E.; Kudin, K. N.; Staroverov, V. N.; Kobayashi, R.; Normand, J.; Raghavachari, K.; Rendell, A.; Burant, J. C.; Iyengar, S. S.; Tomasi, J.; Cossi, M.; Rega, N.; Millam, J. M.; Klene, M.; Knox, J. E.; Cross, J. B.; Bakken, V.; Adamo, C.; Jaramillo, J.; Gomperts, R.; Stratmann, R. E.; Yazyev, O.; Austin, A. J.; Cammi, R.; Pomelli, C.; Ochterski, J. W.; Martin, R. L.; Morokuma, K.; Zakrzewski, V. G.; Voth, G. A.; Salvador, P.; Dannenberg, J. J.; Dapprich, S.; Daniels, A. D.; Farkas, O.; Foresman, J. B.; Ortiz, J. V.; Cioslowski, J.; Fox, D. J. Gaussian 09, revision D.01; Gaussian, Inc.: Wallingford, CT, 2009.

For Table of Contents Only

Graphic

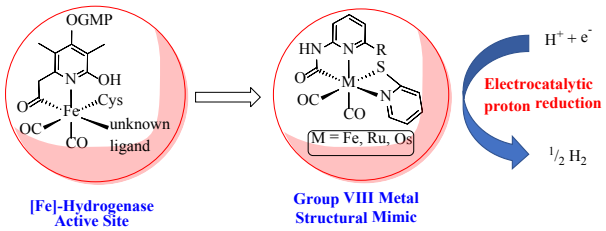

Synopsis

A complete set of structural mimics of the [Fe]-hydrogenase for the group VIII metals has been prepared. They exist as isomers with relative stability which depended on both the identity of the metal and ligand steric effects, in particular, substitution at the 6-position of the carbamoyl pyridine ligand. The complexes are also active electrocatalysts for proton reduction.